High-Speed Photodetector With Simultaneous Electrical Power Generation

Luyu Wang, Zhiyang Xie, Beibei Pan, Zhiqi Zhou, Linze Li, Xinbo Zou, *Member, IEEE*, Haiming Ji, and Baile Chen, *Senior Member, IEEE*

***Abstract*—We demonstrate a novel 850 nm high-speed photodetector for simultaneous high-speed data acquisition and electrical power generation from the optical signal. The device is based on GaAs/AlGaAs modified uni-traveling carrier photodetector (MUTC-PD). Compared with the traditional p-i-n photodetector with the same absorber thickness, the MUTC device sustains a high 3 dB bandwidth of 11.9 GHz and a power conversion efficiency of 38.5% under a forward bias of +0.7 V. This outstanding performance is achieved by first adopting the MUTC structure on LPC devices. The device is expected to have applications for simultaneous lightwave information and power transfer. Our approach extends the high-speed detection to the forward bias region and may provide a potential solution for next-generation combined power and data transceiver modules.**

***Index Terms*—High-speed photodetectors, laser power converters, optical power transmission, photovoltaic, SWIPT.**

I. Introduction

MODERN data centers and high-performance computing (HPC) systems increasingly rely on optical interconnects (OI) for high-speed short-haul optical communication at 850 nm band, which reduces the power-hungry microwave components and cable bulk with frequency dependent losses, crosstalk, and frequency resonance effects [1], [2], [3]. However, the recent acceleration in network bandwidth has boosted the data center's power consumption to more than 100 MW, which raises increasing public concerns about climate change and environmental issues [4], [5].

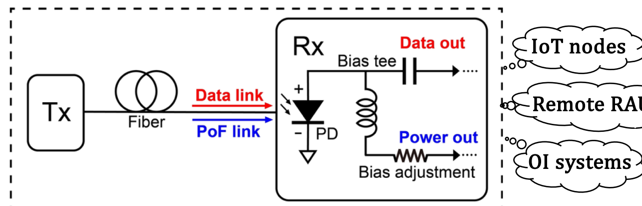

Fig. 1. Schematic diagram of the radio and power over fiber system.

Power-over-fiber (PoF) is an attractive approach for delivering electric power by using optical fibers and a photovoltaic (PV) receiver (Rx) in the Radio-over-fiber (RoF) system [6]. The concept of PoF has also been applied to many scenarios like feeding some reconfigurable elements in optical access networks [7] and optically powering remote antenna units (RAUs) [8], [9], which is beneficial in terms of system simplicity and cost. Therefore, it is appealing to integrate the optical power link to the massive optical data link of the OI system to increase the power efficiency and reduce system complexity. T. Umezawa et al. reported a novel uni-traveling carrier photodetector (UTC PD) under a forward bias to convert data and power simultaneously in a 100-GHz radio and power over fiber transmission system at 1.55 μm [9], [10], where the generated power from the UTC PD was applied to drive the gate bias (in μW level) of an InP PHEMT amplifier. The complexity and power efficiency of the OI systems can be greatly improved by introducing this kind of high-speed photoconverter operating in photovoltaic mode on the receiver side. An in-home networking scenario of simultaneous multi Gbit/s data transmission and energy delivery for Internet of Things (IoT) nodes (in tens to hundreds of μW range) over the same plastic optical fiber was discussed in the reference [11], [12], where an avalanche photodetector (APD) and PV cell were used for data detection and power generation. Therefore, power-harvesting and high-speed photodetectors in PV mode offer great potential for alternative energy production in Rx modules by generating electrical power and data transmission simultaneously. A Schematic diagram of the radio and power over fiber system and the application of scenarios of LPC devices is illustrated in Fig. 1 [9], [10], [11], where the operation bias of the PV cell can be fine-tuned by an external bias adjustment circuit [13], [14].

Manuscript received 3 August 2022; revised 14 September 2022 and 14 October 2022; accepted 19 October 2022. Date of publication 25 October 2022; date of current version 15 January 2023. This work was supported in part by the National Key Research and Development Program of China under Grant 2018YFB2201000, in part by the National Natural Science Foundation of China under Grant 61975121, and in part by the Double First-Class Initiative Fund of ShanghaiTech University. *(Luyu Wang and Zhiyang Xie contributed equally to this work.) (Corresponding author: Baile Chen.)*

Luyu Wang and Zhiyang Xie are with the School of Information Science and Technology, ShanghaiTech University, Shanghai 201210, China, also with the Shanghai Institute of Microsystem and Information Technology, Chinese Academy of Sciences, Shanghai 200050, China, and also with the University of Chinese Academy of Sciences, Beijing 100049, China (e-mail: wangly4@shanghaitech.edu.cn; xiezhy@shanghaitech.edu.cn).

Beibei Pan, Zhiqi Zhou, Linze Li, Xinbo Zou, and Baile Chen are with the School of Information Science and Technology, ShanghaiTech University, Shanghai 201210, China, and also with the Shanghai Engineering Research Center of Energy Efficient and Custom AI IC, Shanghai 201210, China (e-mail: panbb@shanghaitech.edu.cn; zhouzq@shanghaitech.edu.cn; lilz@shanghaitech.edu.cn; zouxb@shanghaitech.edu.cn; chenbl@shanghaitech.edu.cn).

Haiming Ji is with the University of Chinese Academy of Sciences, Beijing 100049, China (e-mail: jhm@semi.ac.cn).

Color versions of one or more figures in this article are available at https://doi.org/10.1109/JLT.2022.3216839.

Digital Object Identifier 10.1109/JLT.2022.3216839

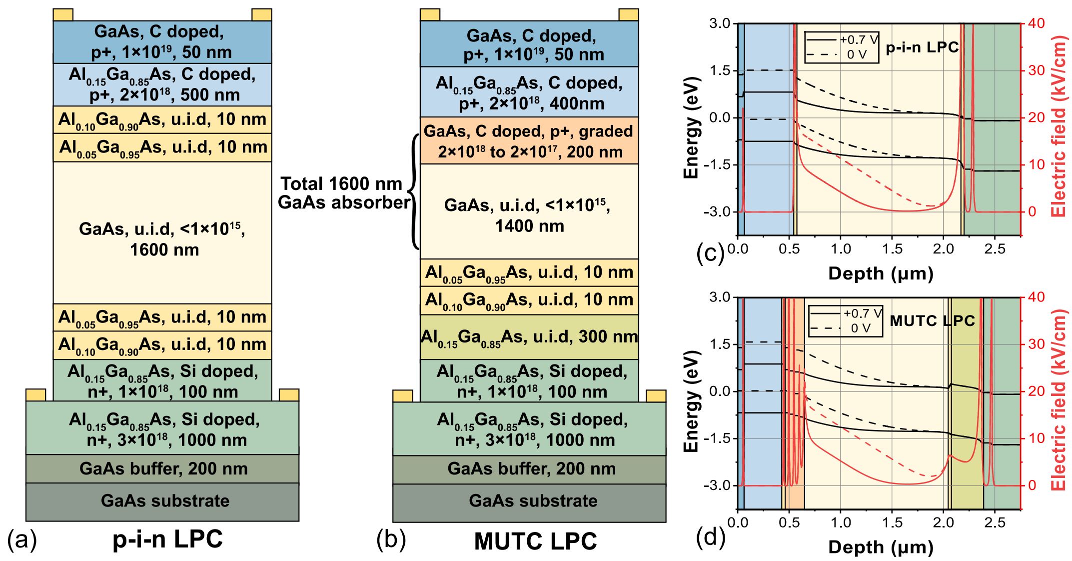

Fig. 2. The epitaxial structures of the top-illuminated (a): p-i-n and (b): MUTC LPCs. The simulated band diagram and electric field under 0 V and +0.7 V bias of (c): p-i-n and (d): MUTC LPCs.

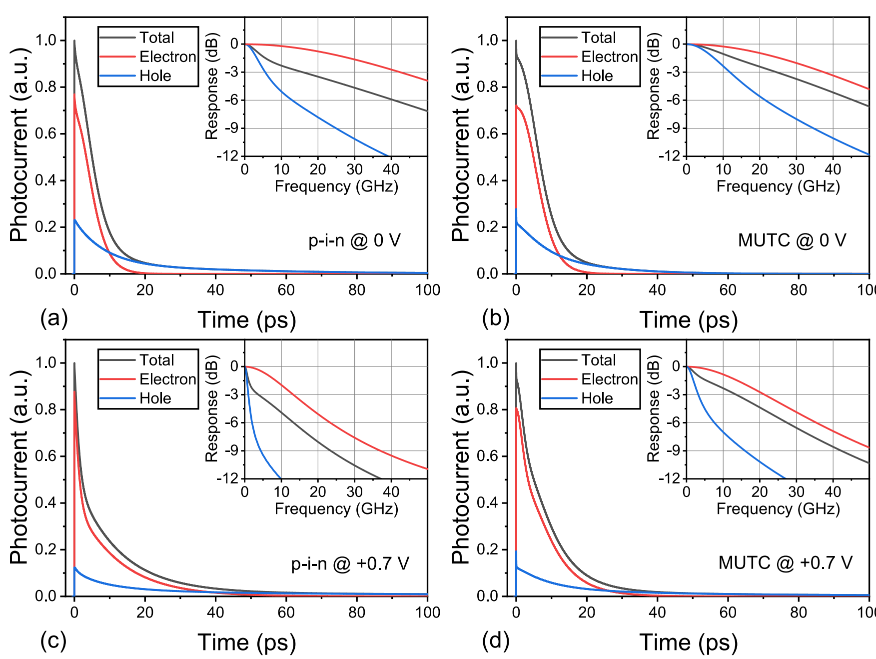

Fig. 3. The simulated impulse currents of p-i-n and MUTC devices under (a)-(b): zero bias and (c)-(d): +0.7 V bias. The insets show the calculated frequency response.

Generally, there are two approaches to realizing an integrated power and data receiving device: (1) implementing single-junction PV cells as a data receiver [15], [16], and (2) enhancing the power efficiency of the III–V-based high-speed photodetector operating under a forward bias. The conversion efficiency of the state-of-the-art laser power converters (LPC) using single-junction PV cells is 55% at 37 W/cm^2 [17] and 60% at 10 W/cm^2 [18], [19], which means high conversion efficiency can be easily achieved by PV cells. However, the high-speed performances of single-junction PV cells are significantly restricted by the low bandwidth of the simple p-n junction. A high data rate of 1 Gbit/s was demonstrated with a GaAs-based 850 nm vertical-cavity surface-emitter laser (VCSEL) and a GaAs PV cell [16]. The 3dB bandwidth and conversion efficiency of the PV cell is 24.5 MHz and 41.7%.

As for III–V-based high-speed photodetectors, traditional p-i-n photodetectors typically need to operate under a reverse bias for high-speed operation. To generate electrical power instead of consuming electrical power for energy harvesting applications, the devices should operate under a forward bias. However, it is challenging for traditional p-i-n photodiodes to maintain a high operation bandwidth under a forward bias, due to the slow

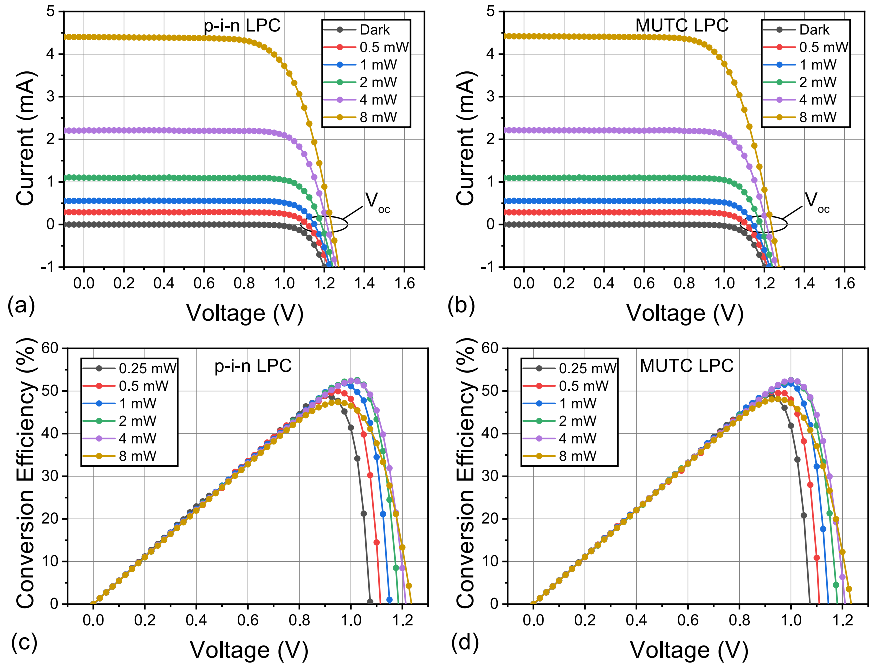

Fig. 4. Measured photocurrents under different optical powers versus forward bias voltages of (a): p-i-n and (b): MUTC LPCs. The power conversion efficiency of (c): p-i-n and (d): MUTC LPCs.

hole transport under the reduced internal built-in electrical field. The uni-traveling-carrier photodiode (UTC-PDs) can overcome the slow hole transport by using a p-type absorption layer, where the photogenerated hole can relax within the dielectric relaxation time [20], [21], [22]. In UTC-PDs, only the electron transit time dominates the total carrier transit time, thus they are expected to have a higher speed than traditional p-i-n photodiodes, especially under the reduced internal built-in electrical field [23], [24]. Therefore, UTC-PD is a potential solution for generating (instead of consuming) DC electrical power during high-speed data transmission in optical interconnects systems given the fast electron transport. At 850 nm wavelength, F. M. Kuo et al. reported a cascade GaAs/AlGaAs LPC structure, with an error-free 10 Gbit/s data detection rate and 21.1% optical-to-electrical DC power conversion efficiency under +1 V bias [25], [26]. J. Shi et al. reported a GaAs/$In_{0.5}Ga_{0.5}P$ device with the undercut mesa structure, which achieved a 3 dB bandwidth of 9 GHz under +0.8 V bias, with a power conversion efficiency of 15% [27]. However, the devices in these works adapted very thin absorbers and depleted intrinsic layers (hundreds of nanometers), which results in a relatively low conversion efficiency and RC-time-limited bandwidth.

In this work, we demonstrate a GaAs/AlGaAs high-speed laser power converter based on the modified uni-traveling-carrier photodetector (MUTC-PD) structure, which can exhibit high DC conversion efficiency and sustain a high-speed data transmission under a forward bias operation. Under +0.7 V bias, the device can achieve optimized performance with a high optical-to-electrical conversion efficiency of 38.5% and 3dB bandwidth of 11.9 GHz, with a data rate of 25.8 Gbit/s. The MUTC LPCs outperform all other similar devices demonstrated so far, in terms of the 3dB bandwidth. The devices in this work also show a conversion efficiency comparable to that of conventional PV cells. The performance of the devices is characterized in detail under a forward bias by comparing with the traditional p-i-n PD with the same thickness of GaAs absorber, along with the equivalent circuit model.

II. Device Structure

Fig. 2(a) and (b) show the epitaxial structures of the designed GaAs/AlGaAs based top-illuminated p-i-n and MUTC photodetectors. The samples were grown on the semi-insulating GaAs substrate by the metal-organic chemical vapor deposition (MOCVD) system. The detailed material growth and device fabrication steps of the MUTC PD are reported in reference [28]. A similar procedure was conducted on the p-i-n device. The GaAs absorber of the MUTC device consists of a 1400 nm thick un-intentionally doped GaAs layer and four 50 nm p-type undepleted absorber layers with step grading doping profile, which creates a quasi-electric field that aids electron transport. The photogenerated holes in the p-type GaAs of the MUTC device can respond within the dielectric relaxation time as the majority carriers, while the electrons can achieve a high instantaneous velocity with the self-induced electric field and the graded accepter doping (see Fig. 2(d)) [29]. Moreover, the p-doped GaAs layer can decrease the ratio of absorption and the transport distance of holes in the u.i.d GaAs absorber. Considering the low electric field profile under forward bias and laser illumination (see Fig 2(c)-(d)), the holes with much lower mobility could not be accelerated to a high velocity. As the $Al_{0.15}Ga_{0.85}As$ is transparent to the 850 nm light source, the depleted intrinsic AlGaAs layer would not give rise to an additional traveling time of slow holes to p-region, but was designed to decrease

TABLE I
PARAMETERS OF GaAs IN THE SIMULATION MODEL

Symbol	Parameter	Value	Unit
α	Absorption coefficient	1×10^4	cm^{-1}
μ_e	Electron mobility	8500	$cm^2 \cdot V^{-1} \cdot s^{-1}$
μ_h	Hole mobility	500	$cm^2 \cdot V^{-1} \cdot s^{-1}$
D_e	Electron diffusion coefficient	220	$cm^2 \cdot s^{-1}$
D_h	Hole diffusion coefficient	13	$cm^2 \cdot s^{-1}$
V_{esat}	Electron saturation velocity	1×10^7	$cm \cdot s^{-1}$
V_{hsat}	Hole saturation velocity	1×10^7	$cm \cdot s^{-1}$
τ_e	Electron lifetime	1×10^{-9}	s
τ_h	Hole lifetime	2×10^{-8}	s
ε_r	Dielectric constant	12.9	-

the junction capacitance and RC time of the device. Thus, the total transport distance of slow holes is shorter than that of p-i-n devices. Compared with traditional PV cells of p-n junctions and UTC devices, by properly designing the thickness ratio of p-type GaAs and intrinsic GaAs of the MUTC LPC, the transit time of electrons and holes can be balanced. Moreover, the additional intrinsic GaAs absorber can increase the power conversion efficiency, and reduce the impact of the RC time on the bandwidth together with the 300 nm intrinsic AlGaAs layer. Therefore, MUTC devices can exhibit better high-speed performance than UTC devices even with a thicker absorber. On the other hand, as the GaAs absorption layer of both MUTC and p-i-n LPCs have the same thickness of 1.6 μm, they could have a similar optical-to-electrical power conversion efficiency.

The bandwidth simulation based on the small-signal impulse response was used to verify the design in this work [30], [31], where the basic parameters in the model are shown in Table I. The simulated normalized impulse response of hole, electron, and total current versus time of devices under 0 V and +0.7 V bias are shown in Fig. 3. It is shown that the FWHM of hole current of p-i-n and MUTC device under zero bias are about 7.3 ps and 5.8 ps, respectively. The corresponding 3dB bandwidth can be determined by the Fourier Transform of the impulse currents, as shown in the insets of Fig. 3. The transit-time-limited bandwidth of p-i-n and MUTC device is 15.8 GHz and 24.6 GHz under zero bias, respectively. As the bias rises to +0.7 V, the bandwidth of total current of the p-i-n and MUTC devices decreases to 3.8 GHz and 13.6 GHz. Therefore, the MUTC device has a much better transit-time-limited bandwidth performance than the p-i-n device owing to the faster hole response in the p-doped GaAs layer.

III. MEASUREMENT RESULTS AND DISCUSSION

A. I-V Characteristics and Conversion Efficiency

The conversion efficiency of the LPCs is defined as $\eta = \frac{I \times V}{P_{in}} \times 100\%$ [32]. The current versus bias voltage (I-V) characteristics at room temperature of the p-i-n and MUTC LPCs were measured by a source meter and an 852 nm wavelength DFB laser connected with lens fiber. The dark currents of both LPCs are around 80 μA under +0.7 V, as shown in Fig. 4(a) and (b). The optical-to-electrical power conversion efficiencies versus bias voltage are shown in Fig. 4(c) and (d), deriving from the I-V characteristics. The I-V characteristics of p-i-n and MUTC devices are almost identical, which indicates that the conversion efficiency is dominated by the thickness of the GaAs absorber. The conversion efficiency under +0.7 V and +0.8 V is 38.6% and 45.2%, respectively, higher than that of the GaAs-based LPC (15% under +0.8 V) reported in reference [27]. Under 2 mW optical power, both devices reach a maximum conversion efficiency of 52.5% under +1.025 V bias, which is quite high even for dedicated GaAs LPCs. The maximum output electrical power of around 4 mW under +0.95 V bias can be steadily generated with 8 mW optical power injection. This output power level is expected to be sufficient for IoT nodes [11], [12].

The open-circuit voltage (V_{OC}) of an LPC is defined as the available voltage at the zero current point, similar to a solar cell. The Voc versus laser power intensity curves of p-i-n and MUTC LPCs are shown in Fig. 5(a). The V_{OC} increases almost logarithmically with the incident power density, implying that the devices could perform as a concentrator solar cell [33]. Fig. 5(b) shows the maximum conversion efficiencies as a function of laser power density for both devices measured under the forward bias of near +1 V. The efficiencies rise as the power density increases from 0 to 160 W/cm^2, which is equivalent to the total optical power of 2 mW, and then drops slightly as the pumping power further increases.

To investigate the impact of the thickness and background doping level of the u.i.d GaAs on the LPCs and the degradation of the maximum conversion efficiency at high illumination, a simulation of the devices was conducted in the Silvaco TCAD software[34]. Fig. 6(a) shows the relationship of the conversion efficiency and thickness of GaAs absorber under +0.7 V and +1.0 V bias, based on a p-i-n structure with u.i.d GaAs absorber of different background doping concentrations. The result indicates the efficiency of LPC devices significantly depends on the thickness of the absorber. The O-E efficiency also shows little relevance to the background doping concentration, which is due to the large carrier diffusion length of several μm [35], [36]. The simulated conversion efficiencies of the MUTC device are depicted in Fig. 6(b), which agrees well with the measured curves (see Fig. 4(d)).

The simulated electric fields of the p-i-n and MUTC devices with different background doping concentrations under +0.7 V and 1 mW optical power are illustrated in Fig. 7(a) and (b). The depleted region width of devices is subject to the background doping level under forward bias, where a higher concentration would increase the diffusion time of carriers and RC-time of devices. Fig. 7(c) and (d) show the simulated electric fields of the p-i-n and MUTC devices under +1 V and various optical powers. The electric field in the un-intentionally doped GaAs layer is further screened by the space-charge field as the photocurrent increases, which could result in an increase of carrier recombination and contribute to a degradation of maximum conversion efficiency [26]. However, the space-charge effect of MUTC device is less severe as compared to p-i-n device, since

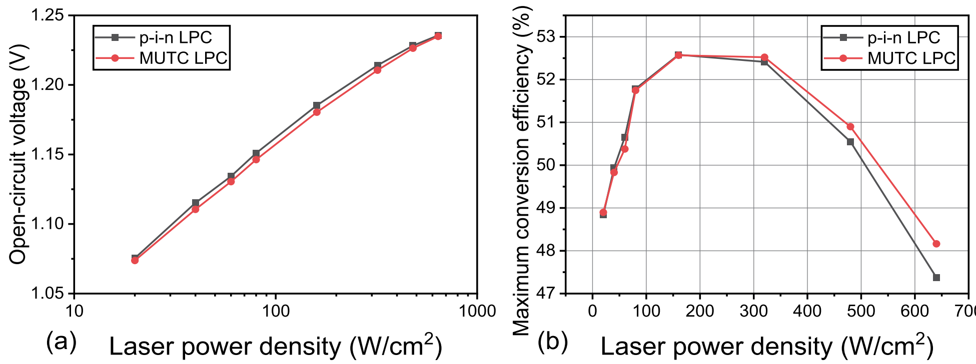

Fig. 5. (a): Open-circuit voltage Voc versus input power intensity. (b): LPC maximum power conversion efficiency versus input power intensity.

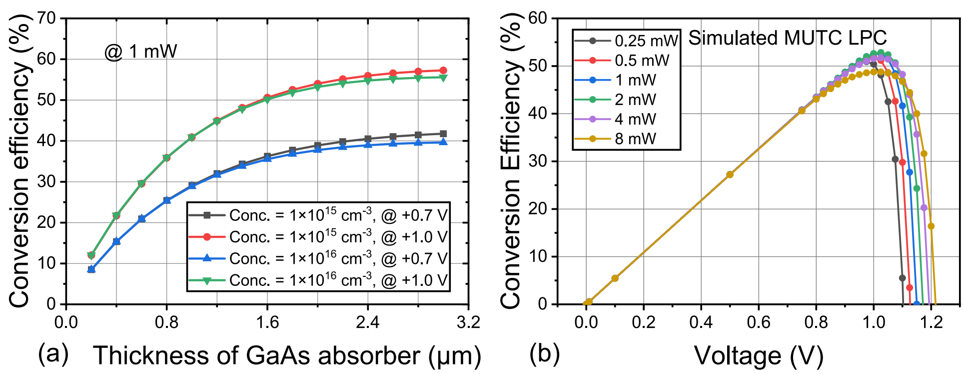

Fig. 6. (a) Simulated power conversion efficiency versus thickness of GaAs absorber of p-i-n device under 1 mW illumination. (b) Simulated power conversion efficiency of the MUTC device.

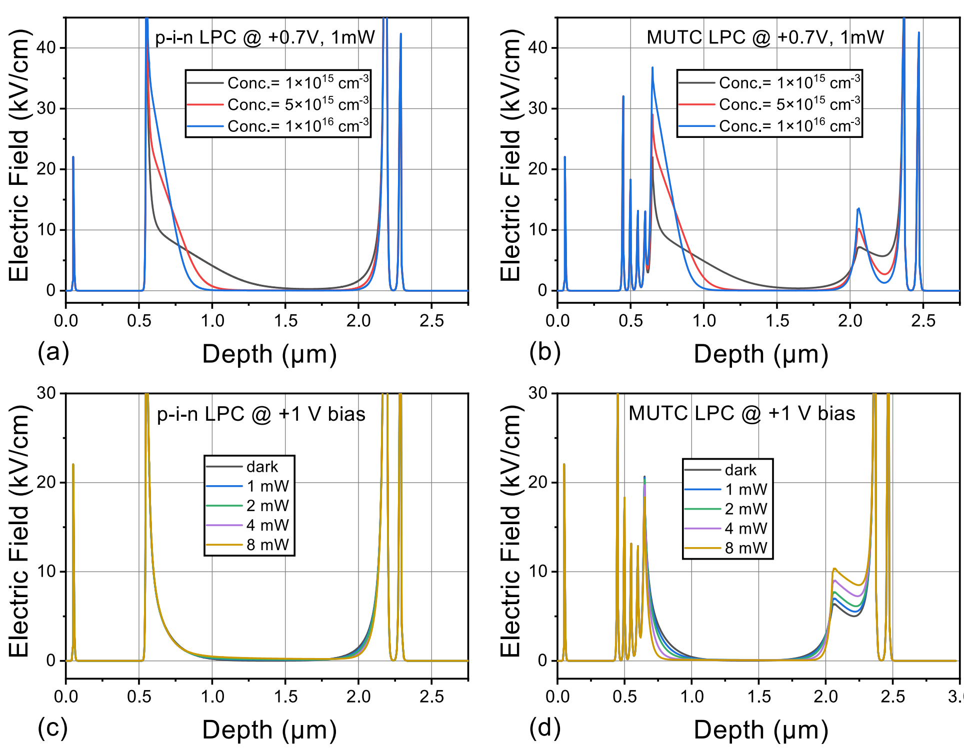

Fig. 7. The simulated electric field profile of the (a): p-i-n device and (b): MUTC device with different intrinsic layers doping levels under 1 mW illumination. The simulated electrical field of the (c): p-i-n device and (d): MUTC device under +1 V bias and various optical power.

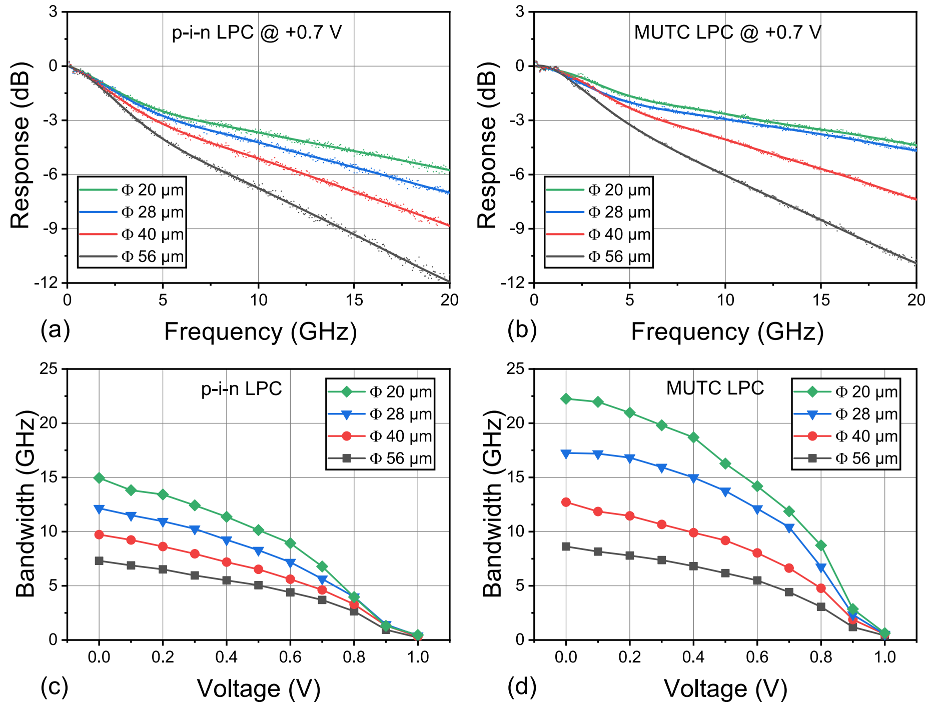

Fig. 8. Frequency response of the (a): p-i-n and (b): MUTC LPCs with different diameters under +0.7 V forward bias. 3dB bandwidth of the (c): p-i-n and (d): MUTC devices with different diameters under 0 V to +1 V forward bias.

the slow hole transport distance in MUTC device is shorter than that of p-i-n device. That is why the conversion efficiency of MUTC device is higher than that of p-i-n device under high illumination as shown in Fig. 5(b).

B. High-speed Characterization

The frequency response of the devices under a forward bias at room temperature was investigated by a calibrated Lightwave Component Analyzer (LCA) system at 852 nm wavelength, which was introduced in reference [28]. Fig. 8(a), (b) show the measured frequency response of the p-i-n and MUTC LPCs with different diameters under +0.7 V forward bias and a fixed photocurrent of 90 μA. The 20 μm and 40 μm MUTC devices exhibit 3dB bandwidths of 11.9 GHz and 6.6 GHz, respectively, larger than the bandwidths of p-i-n devices (6.3 GHz and 4.4 GHz).

The frequency responses of the LPCs under various forward biases from 0 V to +1 V were also conducted. The corresponding 3dB bandwidths are illustrated in Fig. 8(c) and (d). The MUTC devices exhibit larger 3dB bandwidths than the p-i-n devices from the zero-bias to the near open-circuit voltage of +1 V. For both devices, the 3dB bandwidths decline with the increasing forward bias voltage as the electric field in the GaAs absorber region gradually attenuates. The bandwidth performance under +1 V is mainly limited by the diffusion process of carriers in the undepleted region, which occupies most of the u.i.d GaAs absorber (see Fig. 7(c)-(d)). Therefore, the 3dB bandwidth of both LPC devices under +1 V is lower than 1 GHz. As shown in Fig. 8(d), the 20 μm MUTC device can exhibit 3dB bandwidths of 14.2 GHz, 11.9 GHz, and 8.7 GHz under +0.6 V, +0.7 V, and +0.8 V bias, respectively, which is so far the highest bandwidth that single 850 nm photodetectors can achieve in the forward bias region.

In order to investigate the bandwidth limiting factors of the p-i-n and MUTC LPCs, the scattering parameters of devices were measured by a Vector Network Analyzer (VNA). The parameter fitting was conducted in the Advanced Design System (ADS) software with an equivalent circuit model as depicted in Fig. 9(a). In the equivalent circuit model, R_s and L_s represent the series resistance and series inductance. R_j is the junction resistance and C_{PD} is the total capacitance of the LPC, including the parasitic capacitance (C_p), junction capacitance (C_j), and diffusion capacitance (C_d). The diffusion capacitance is parallel with C_j and is caused by the excess minority carriers stored near the depletion region edges when the device is working under a forward bias [37]. Since the intended operating voltage of +0.7 V is lower than the maximum output electrical power point of around +0.95 V, the junction capacitance cannot be neglected [38].

The transit time limitation is approximated by the R_t, C_t, and C_{sc}, where the C_{sc} represents the influence of the space charge effect on frequency response [39]. Region 1 is applied to mimic the frequency response of carrier transit time. Region 2 is used to fit the measured curve of the one-port S-parameter for the extraction of RC-time-limited frequency response. Fig. 9(b) and (c) show the measured and fitted S-parameter (from 50 MHz to 35 GHz) of the 20 μm p-i-n and MUTC devices under +0.6 V, +0.7 V, and +0.8 V bias and a 90 μA output photocurrent. For both devices, the starting point of the S22 trace moves away from the open-circuit point ($Z = \infty$) as the forward bias increases. This phenomenon reflects a reduction of

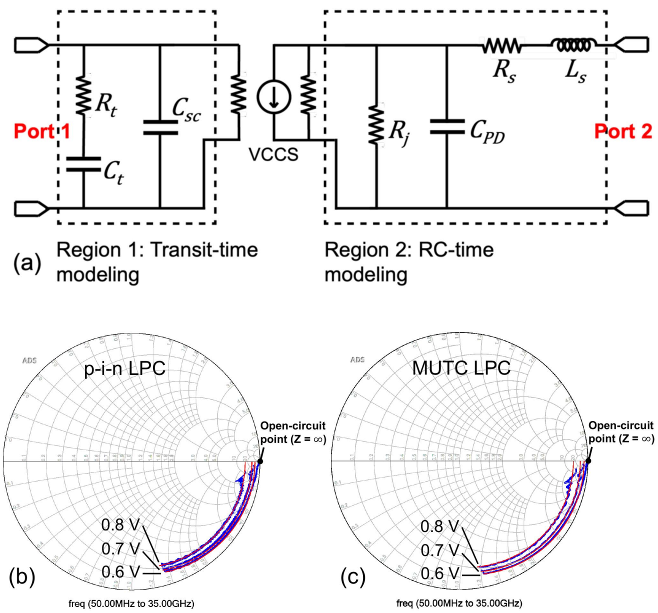

Fig. 9. (a) Equivalent circuit model of the LPCs for S-parameter fitting. Smith chart showing the measured (blue lines) and fitted (red lines) S22 parameters for 20 μm (b): p-i-n and (c): MUTC LPCs under the forward bias voltages of +0.6 V, +0.7 V, and +0.8 V.

TABLE II
FITTING PARAMETERS OF P-I-N LPC

Bias voltage (V)	C_{PD} (fF)	R_j (kΩ)	R_s(Ω)	L_s(pH)
+0.6	62.5	2.6	7.3	21.8
+0.7	63.9	1.6	6.9	14.5
+0.8	67.1	0.8	6.3	0.1

TABLE III
FITTING PARAMETERS OF MUTC LPC

Bias voltage (V)	C_{PD} (fF)	R_j (kΩ)	R_s(Ω)	L_s(pH)
+0.6	67.4	2.6	6.0	23.6
+0.7	68.9	1.7	6.1	20.5
+0.8	72.9	0.8	5.7	1.4

TABLE IV
THE CAPACITANCES OF P-I-N LPC AND MUTC LPC UNDER +0.7V

LPC type	C_p (fF)	C_j (fF)	C_d (fF)	Calculated C_{PD} (fF)	Extracted C_{PD} (fF)	Measured C_{PD} (fF)
p-i-n	38.5	21.9	8.8	69.2	63.9	75.6
MUTC	36.5	20.9	3.1	60.5	68.9	82.8

junction resistance (R_j), which is caused by the increase of the forward conduction current as the forward bias voltage rises. The extracted parameters are summarized in Table II and Table III.

The result of a detailed analysis of device capacitance under +0.7 V is shown in Table IV. A theoretical calculation of C_{PD} is also conducted by determining C_p, C_j, and C_d. The parasitic capacitance (C_p) is determined from the intercept of the linear fit by plotting the measured C_{PD} versus device areas. We define C_j as $C_j = \frac{\varepsilon A}{W_j}$, where W_j is approximate as the length of the intrinsic region. The C_d is determined by $C_d = \frac{\tau I_d}{V_T}$ [40], where τ is the device transit time, I_d is the diffusion current and V_T is the thermal voltage. The results show that the junction capacitance and parasitic capacitance still dominate the total capacitance under +0.7 V bias, and the calculated C_{PD} is consistent with the extracted C_{PD}, as well as the measured C_{PD} under +0.7 V by a semiconductor device analyzer at 1 MHz. The value of the extracted and measured capacitance of the MUTC device is a bit larger under forward bias, which may be due to the slightly higher background doping levels of u.i.d GaAs and AlGaAs layers, as discussed in Section A.

After the parameters of the RC-time model are determined, the transit-time-limited frequency responses and parameters in the circuit model of transit-time are extracted by fitting the polynomial fitting curve of measured frequency response (green curve in Fig. 10(a)-(b)) by using the whole equivalent circuit model (S21) in Fig. 9(a). The measured and extracted curves show a similar trend to the simulation results in Fig. 3. The larger slope of the frequency response at a lower frequency is possibly due to the slow hole transport, while the flat frequency response at a higher frequency beyond about 6 GHz is contributed by the fast electron transport. Fig. 10(a), (b) show the RC-time-limited, transit-time-limited, measured optical-to-electrical, and fitted optical-to-electrical frequency responses of p-i-n and MUTC devices of 20 μm diameter under the forward bias of +0.7 V bias and 90 μA photocurrent. The RC-time-limited bandwidths (f_{RC}), transit-time-limited bandwidths (f_{tr}), and total 3dB bandwidth (f_{3dB}) of p-i-n LPCs are 48.6 GHz, 7.8 GHz, and 6.8 GHz. For the MUTC LPCs, the f_{RC}, f_{tr}, and f_{3dB} are 46.9 GHz, 14.6 GHz, and 11.9 GHz, respectively.

Fig. 10(c) and (d) summarize the f_{RC}, f_{tr}, and f_{3dB} versus forward bias voltages of the 20 μm p-i-n and MUTC LPCs. The carrier transit time contributes to the 3dB bandwidth degradation of both devices with the increasing forward bias voltage. As described in Section II, the designed MUTC LPCs balance the transit distance of photogenerated carriers, whereas the slow holes dominate the bandwidth of p-i-n devices. According to the simulated electric fields of the p-i-n and MUTC LPCs under +0.7 V bias and 90 μA photocurrent shown in Fig. 3(c) and (d), the undepleted region of the MUTC LPCs is narrower than that of the p-i-n LPCs, which aids the transport of photogenerated carriers. Therefore, the MUTC LPCs have superior high-speed performance to the p-i-n LPCs, attributed to the faster transit-time response. It should be also noted that the 3dB bandwidth performance of the MUTC devices can be further improved by reducing the thickness of AlGaAs collector layer, since the 3dB bandwidth of the MUTC device is also limited by the transit time. A properly designed partial-depleted-absorber structure without AlGaAs collector layer may be expected to have better high-speed performance while having a similar power conversion efficiency performance.

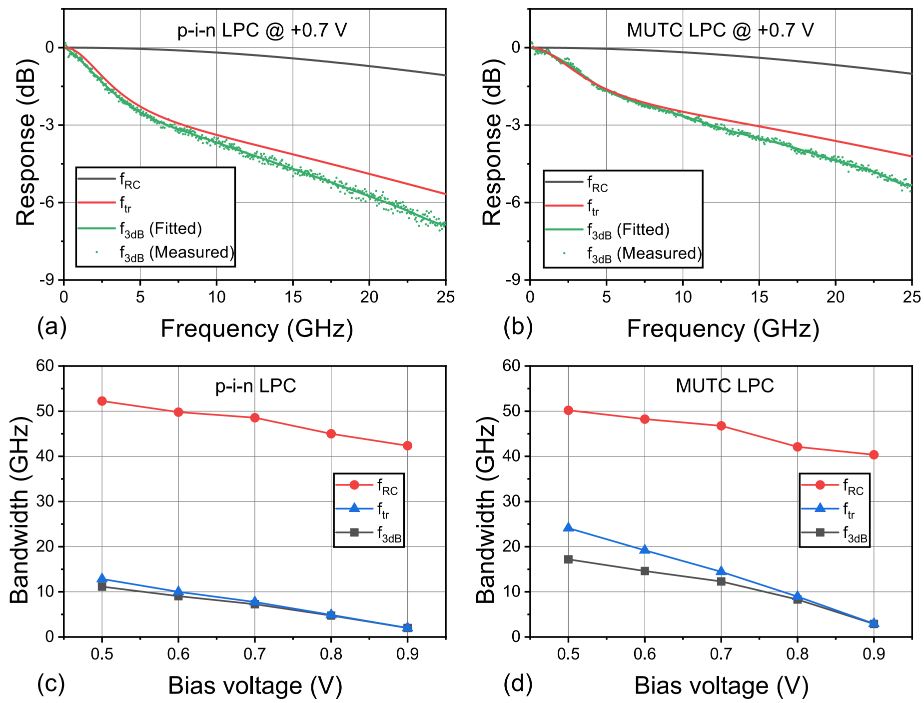

Fig. 10. The RC-time-limited, transit-time-limited, measured, and fitted optical-to-electrical frequency responses of (a): p-i-n and (b): MUTC devices of 20 μm diameter under the forward bias of +0.7 V bias and 90 μA photocurrent. 3dB bandwidth, RC-time-limited bandwidth, and transit-time-limited bandwidth versus forward bias voltages for the 20 μm (c): p-i-n LPC and (d): MUTC LPC.

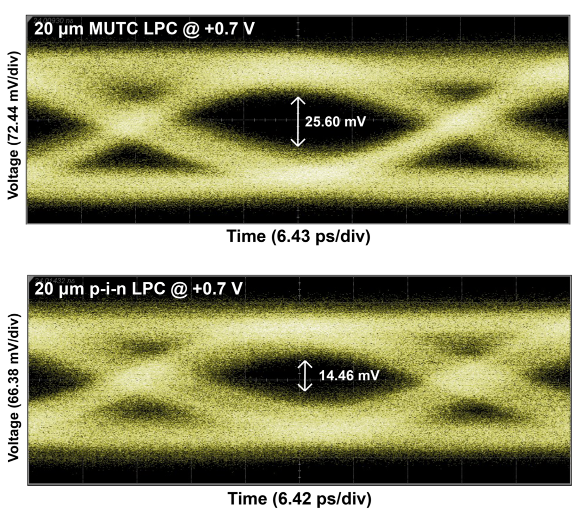

Fig. 11. Eye diagram of the 20 μm MUTC and p-i-n device under +0.7 V forward bias.

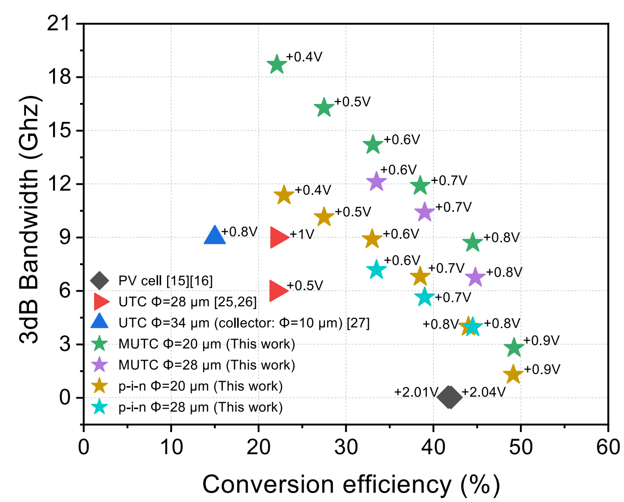

Fig. 12. State-of-the-art performance of the devices for integrated power and data receiving under 850 nm wavelength. The data label indicates the operating voltage.

Fig. 11 shows the eye diagram of the 20 μm MUTC and p-i-n device under +0.7 V bias at the NRZ data rate of 25.8 Gbit/s. The average output photocurrent is about 180 μA. The optical signal was generated by a commercial 850 nm high-speed VCSEL module. The photodiode's output RF signal was amplified by a +23 dB microwave amplifier and then displayed on the real-time sampling oscilloscope. The 2^{10}–1 pseudo-random binary sequence (PRBS) patterns were generated by an arbitrary waveform generator (AWG) as the data source. Compared with p-i-n devices, the MUTC devices exhibit a clearer eye pattern with a larger eye-opening, suggesting that MUTC LPCs are highly promising for realizing simultaneous high-speed detection and power generation.

Key parameters of the various state-of-the-art integrated lightwave power and data receiving devices reported in the literature are compared in Fig. 12. The data label indicates the operating bias where the device can achieve the corresponding 3dB bandwidth and conversion efficiency. In this work, the LPC devices have a balanced performance of high-speed characteristics and high efficiency under +0.7 V bias. Our device outperforms all other approaches demonstrated so far in terms of power conversion efficiency and 3dB bandwidth.

IV. Conclusion

In this work, we demonstrate a GaAs/AlGaAs-based modified uni-traveling-carrier photodetector for simultaneous energy and data collection, which can exhibit high-speed data transmission (11.9 GHz) under a forward bias operation (+0.7 V) with a power conversion efficiency of 38.5%. By comparing the characteristics of MUTC devices with those of conventional p-i-n devices under a forward bias, it is determined that the higher 3 dB bandwidth of MUTC devices is attributed to their faster transit time response. This novel high-speed LPC may provide a potential solution for simultaneous optical data transmission and power generation and is expected to be integrated into the next-generation combined power and data transceiver modules.

Acknowledgment

The authors would like to thank ShanghaiTech University Quantum Device Lab for the device fabrication.

References

[1] A. F. Benner, M. Ignatowski, J. A. Kash, D. M. Kuchta, and M. B. Ritter, "Exploitation of optical interconnects in future server architectures," *IBM J. Res. Develop.*, vol. 49, no. 4.5, pp. 755–775, Jul. 2005.

[2] M. A. Taubenblatt, "Optical interconnects for high-performance computing," *J. Lightw. Technol.*, vol. 30, no. 4, pp. 448–457, Feb. 2012.

[3] D. G. Kam et al., "Is 25 Gb/s on-board signaling viable?," *IEEE Trans. Adv. Packag.*, vol. 32, no. 2, pp. 328–344, May 2009.

[4] Q. Cheng, M. Bahadori, M. Glick, S. Rumley, and K. Bergman, "Recent advances in optical technologies for data centers: A review," *Optica*, vol. 5, no. 11, pp. 1354–1370, 2018.

[5] G. Cook, *How Dirty is Your Data: A look At the Energy Choices That Power Cloud Computing*. Amsterdam, The Netherlands: Greenpeace, 2011.

[6] M. Matsuura, "Recent advancement in power-over-fiber technologies," *Photonics*, vol. 8, no. 8, 2021, Art. no. 335.

[7] K. Wang, Y. Bi, A. S. Gowda, and L. G. Kazovsky, "Bidirectional quasi-passive reconfigurable (Bi-QPAR) remote node for future optical access networks," *J. Lightw. Technol.*, vol. 35, no. 11, pp. 2109–2117, Jun. 2017.

[8] D. Wake, A. Nkansah, N. J. Gomes, C. Lethien, C. Sion, and J.-P. Vilcot, "Optically powered remote units for radio-over-fiber systems," *J. Lightw. Technol.*, vol. 26, no. 15, pp. 2484–2491, Aug. 2008.

[9] T. Umezawa, P. T. Dat, K. Kashima, A. Kanno, N. Yamamoto, and T. Kawanishi, "100-GHz radio and power over fiber transmission through multicore fiber using optical-to-radio converter," *J. Lightw. Technol.*, vol. 36, no. 2, pp. 617–623, Jan. 2018.

[10] T. Umezawa et al., "100-GHz fiber-fed optical-to-radio converter for radio-and power-over-fiber transmission," *IEEE J. Sel. Topics Quantum Electron.*, vol. 23, no. 3, May/Jun. 2017, Art. no. 3800508.

[11] F. M. Al-Zubaidi, D. S. Montero, and C. Vázquez, "SI-POF supporting power-over-fiber in multi-Gbit/s transmission for in-home networks," *J. Lightw. Technol.*, vol. 39, no. 1, pp. 112–121, Jan. 2021.

[12] P. H. P. Wang, C. Zhang, H. Yang, D. Bharadia, and P. P. Mercier, "20.1 A 28 μW IoT tag that can communicate with commodity wifi transceivers via a single-side-band QPSK backscatter communication technique," in *Proc. IEEE Int. Solid- State Circuits Conf.*, 2020, pp. 312–314, doi: 10.1109/ISSCC19947.2020.9063133.

[13] B. Subudhi and R. Pradhan, "A comparative study on maximum power point tracking techniques for photovoltaic power systems," *IEEE Trans. Sustain. Energy*, vol. 4, no. 1, pp. 89–98, Jan. 2013.

[14] W.-H. Shin, S.-H. Yang, D.-H. Kwon, and S.-K. Han, "Self-reverse-biased solar panel optical receiver for simultaneous visible light communication and energy harvesting," *Opt. Exp.*, vol. 24, no. 22, pp. A1300–A1305, 2016.

[15] J. Fakidis, S. Videv, H. Helmers, and H. Haas, "0.5-Gb/s OFDM-based laser data and power transfer using a GaAs photovoltaic cell," *IEEE Photon. Technol. Lett.*, vol. 30, no. 9, pp. 841–844, May 2018.

[16] J. Fakidis, H. Helmers, and H. Haas, "Simultaneous wireless data and power transfer for a 1-Gb/s GaAs VCSEL and photovoltaic link," *IEEE Photon. Technol. Lett.*, vol. 32, no. 19, pp. 1277–1280, Oct. 2020.

[17] E. Oliva, F. Dimroth, and A. Bett, "GaAs converters for high power densities of laser illumination," *Prog. Photovolt.: Res. Appl.*, vol. 16, no. 4, pp. 289–295, 2008.

[18] V. Khvostikov et al., "Photovoltaic laser-power converter based on AlGaAs/GaAs heterostructures," *Semiconductors*, vol. 50, no. 9, pp. 1220–1224, 2016.

[19] B. Roycroft, M. Baskaran, D. McMahon, and B. Corbett, "Laser to laser power conversion with remote signaling," *Opt. Exp.*, vol. 29, no. 11, pp. 16611–16618, May 2021, doi: 10.1364/OE.423338.

[20] T. Ishibashi and H. Ito, "Uni-traveling-carrier photodiodes," *J. Appl. Phys.*, vol. 127, 2020, Art. no. 3.

[21] T. Ishibashi et al., "InP/InGaAs uni-traveling-carrier photodiodes," *IEICE Trans. Electron.*, vol. 83, no. 6, pp. 938–949, 2000.

[22] T. Ishibashi, S. Kodama, N. Shimizu, and T. Furuta, "High-speed response of uni-traveling-carrier photodiodes," *Japanese J. Appl. Phys.*, vol. 36, no. 10, pp. 6263–6268, Oct. 1997, doi: 10.1143/jjap.36.6263.

[23] J. Huang, Z. Xie, Y. Chen, J. E. Bowers, and B. Chen, "High speed mid-wave infrared uni-traveling carrier photodetector," *IEEE J. Quantum Electron.*, vol. 56, no. 4, Aug. 2020, Art. no. 4000807.

[24] J. Huang et al., "High-speed mid-wave infrared uni-traveling carrier photodetector based on InAs/InAsSb type-II superlattice," *IEEE Electron Device Lett.*, vol. 43, no. 5, pp. 745–748, May 2022, doi: 10.1109/LED.2022.3163660.

[25] F.-M. Kuo, S.-S. Lo, C.-L. Pan, and J.-W. Shi, "Cascade laser power converter for simultaneous 10 gbps data detection and efficient optical-to-electrical dc power generation," in *Proc. Opt. Fiber Commun. Conf. Expo. Nat. Fiber Optic Engineers Conf.*, 2011, pp. 1–3.

[26] J.-W. Shi, F. M. Kuo, C.-S. Yang, S. S. Lo, and C.-L. Pan, "Dynamic analysis of cascaded laser power converters for simultaneous high-speed data detection and optical-to-electrical DC power generation," *IEEE Trans. Electron Devices*, vol. 58, no. 7, pp. 2049–2056, Jul. 2011.

[27] J.-W. Shi et al., "GaAs/$In_{0.5}Ga_{0.5}P$ laser power converter with undercut mesa for simultaneous high-speed data detection and DC electrical power generation," *IEEE Electron Device Lett.*, vol. 33, no. 4, pp. 561–563, Apr. 2012.

[28] Z. Xie, Z. Zhou, L. Li, Z. Deng, H. Ji, and B. Chen, "High-speed 850 nm photodetector for zero-bias operation," *IEEE J. Sel. Topics Quantum Electron.*, vol. 28, no. 2, Mar./Apr. 2022, Art. no. 3801007.

[29] T. Ishibashi, Y. Muramoto, T. Yoshimatsu, and H. Ito, "Unitraveling-carrier photodiodes for terahertz applications," *IEEE J. Sel. Topics Quantum Electron.*, vol. 20, no. 6, pp. 79–88, Nov./Dec. 2014, Art. no. 3804210.

[30] Y.-L. Huang, "Nonlinear saturation behaviors of high-speed pin photodetectors," *J. Lightw. Technol.*, vol. 18, no. 2, pp. 203–212, Feb. 2000.

[31] N. Debbar, "Theoretical study of the DC and transient characteristics of a lateral schottky barrier photodiode for application as high-speed photodetector," *Int. J. Numer. Modelling: Electron. Netw., Devices Fields*, vol. 29, no. 2, pp. 333–342, 2016.

[32] S. Fonash, *Solar Cell Device Physics*. New York, NY, USA: Elsevier, 2012.

[33] J. Schubert, E. Oliva, F. Dimroth, W. Guter, R. Loeckenhoff, and A. Bett, "High-voltage GaAs photovoltaic laser power converters," *IEEE Trans. Electron Devices*, vol. 56, no. 2, pp. 170–175, Feb. 2009.

[34] "Atlas user's manual," in *Silvaco International Software*. Santa Clara, CA, USA: Silvaco, 2018. [Online]. Available: https://silvaco.com/

[35] D. Wight, P. Oliver, T. Prentice, and V. Steward, "Diffusion lengths in p-type MOCVD GaAs," *J. Cryst. Growth*, vol. 55, no. 1, pp. 183–191, 1981.

[36] C. Hwang, "Doping dependence of hole lifetime in n-type GaAs," *J. Appl. Phys.*, vol. 42, no. 11, pp. 4408–4413, 1971.

[37] S. M. Sze and K. K. Ng, *Physics of Semiconductor Devices*. New Yor, NY, USA, USA: Wiley, 2006, pp. 77–133.

[38] G. Friesen and H. Ossenbrink, "Capacitance effects in high-efficiency cells," *Sol. Energy Mater. Sol. Cells*, vol. 48, no. 1–4, pp. 77–83, 1997.

[39] W. CHIU, "A bias-dependent equivalent-circuit model of high performance evanescently coupled photodiode with partially p-doped absorption layer," in *Proc. Extended Abstr. Int. Conf. Solid State Devices Mater.*, 2005, pp. 344–345.

[40] A. H. Chang, A.-T. Avestruz, and S. B. Leeb, "Capacitor-less photovoltaic cell-level power balancing using diffusion charge redistribution," *IEEE Trans. Power Electron.*, vol. 30, no. 2, pp. 537–546, Feb. 2015.